Fronteiras: Journal of Social, Technological, and Environmental Science
http://periodicos.unievangelica.edu.br/fronteiras/
ISSN 2238-8869

Article

Adsorption of Anionic Dyes on Mg/Fe Double Lamellar Hydroxide: An Environmentally Viable Approach

Fernando Carlos Gonçalves Murga[1], Sérgio Botelho de Oliveira[2], Renato Rosseto[3]

[1] PhD student in Chemistry. State University of Goiás. ORCID: 0000-0003-4736-092X. Email: murgameteoro45@gmail.com

[2] Postdoctoral Fellow in Materials and Catalysts. Federal Institute of Goiás. ORCID: 0000-0003-0961-938X. Email: dr_botelho@yahoo.com.br

[3] Postdoctoral Fellow in Lipids and Derivatives and Bioorganic Chemistry. State University of Goiás. ORCID: 0000-0003-4256-9062. Email: renato.rosseto@ueg.br

ABSTRACT

The intensive use of synthetic dyes in industrial processes and the resulting improper disposal of effluents are directly related to the degradation of water quality and increased toxicity in aquatic ecosystems. These compounds alter physical-chemical parameters, such as pH, turbidity, and dissolved oxygen, and affect the dynamics of biological communities, compromising the ecological balance of water bodies. The present study employed the adsorption technique, using Mg^{2+}/Fe^{3+} Double Lamellar Hydroxide (DLH) as an adsorbent material for the removal of the anionic dyes methyl orange and orange G. The adsorbent was characterized by Fourier transform infrared spectroscopy (FTIR), scanning electron microscopy coupled with energy dispersive spectroscopy (SEM/EDS), thermogravimetric analysis (TGA), and X-ray diffraction (XRD). The crystallographic organization of the adsorbent is consistent with the diffraction patterns for an HDL. Adsorption occurred on a rough, irregular surface of stacked plate flakes, which increased the contact area between the dyes and the HDL. Infrared absorption was observed at 1232–1153 cm^{-1}, characteristic bands of C-N bond stretching and the presence of $R\text{-}SO_3^-$ species of the dyes in the solid. Thermogravimetric analyses indicate a greater loss of mass above 380 °C, characteristic of the binding of carbonate ions from the adsorbent with chemical species or groups from the methyl orange dye. Analysis of the pH_{PCZ} associated with the MF41 structure suggests that if the pH of the solution is lower than the pH_{PCZ} (solution pH < 7.45), the surface of the adsorbent will be positively charged, increasing and favoring the adsorption of negatively charged dyes. Adsorption studies showed rapid kinetics, more consistent with the pseudo-second-order model, L-type isotherm, with equilibrium around 150 minutes. The data suggest a combined effect between physisorption and chemisorption of dyes on the adsorbent. HDL demonstrated efficiency in the adsorption of anionic dyes from model aqueous solutions, highlighting its potential as an adsorbent material in effluent treatment technologies.

Keywords: adsorption; anionic clay; chemisorption; environmental remediation.

RESUMO

O uso intensivo de corantes sintéticos em processos industriais e o consequente descarte inadequado de efluentes estão diretamente relacionados à degradação da qualidade da água e ao aumento da toxicidade em ecossistemas aquáticos. Esses compostos alteram parâmetros físico-químicos, como pH, turbidez e oxigênio dissolvido, e afetam a dinâmica das comunidades biológicas, comprometendo o equilíbrio ecológico dos corpos hídricos. O presente estudo empregou a técnica de adsorção, utilizando Hidróxido Duplo Lamelar (HDL) de Mg^{2+}/Fe^{3+} como material adsorvente para a remoção dos corantes aniônicos alaranjado de metila e orange G. O adsorvente foi caracterizado por espectroscopia vibracional no infravermelho médio com transformada de Fourier (FTIR), microscopia eletrônica de varredura acoplada com espectroscopia de energia dispersiva (MEV/EDS), análise termogravimétrica (TGA) e difração de raios X (DRX). A organização cristalográfica do adsorvente está em conformidade com os padrões de difração para um HDL. A adsorção ocorreu sob uma superfície rugosa, irregular, de flocos em placa empilhada, o que proporcionou o aumento da área de contato entre os corantes e o HDL. Observou-se que a absorção no infravermelho ocorreu em 1232 – 1153 cm^{-1}, bandas características do estiramento da ligação C-N e da presença de espécies do tipo $R\text{-}SO_3^-$ dos corantes no sólido. As análises termogravimétricas indicam uma perda maior de massa acima de 380 ºC de temperatura, característica da ligação de íons carbonato do adsorvente com espécies químicas ou grupos do corante alaranjado de metila. A análise do pH_{PCZ} associado à estrutura do MF41 sugere que se o pH da solução for menor do que o pH_{PCZ} (pH solução < 7,45), a superfície do adsorvente ficará carregada

Submission: August 8, 2025 Accepted: December 3, 2025 Publication: 19/12/2025

v.14, n.4, 2025 • p. 1-24. • DOI http://dx.doi.org/10.21664/2238-8869.2025v14i4.8294

positivamente, aumentando e favorecendo a adsorção de corantes com carga negativa. Os estudos de adsorção mostraram uma cinética rápida, mais ajustada ao modelo de pseudo-segunda ordem, isoterma do tipo L, com equilíbrio em torno de 150 minutos. Os dados sugerem um efeito combinado entre fisiossorção e quimissorção dos corantes no adsorvente. O HDL demonstrou eficiência na adsorção dos corantes aniônicos a partir de soluções aquosas modelo, evidenciando seu potencial como material adsorvente em tecnologias de tratamento para efluentes.
Palavras-chave: adsorção; argila aniônica; quimissorção; remediação ambiental.

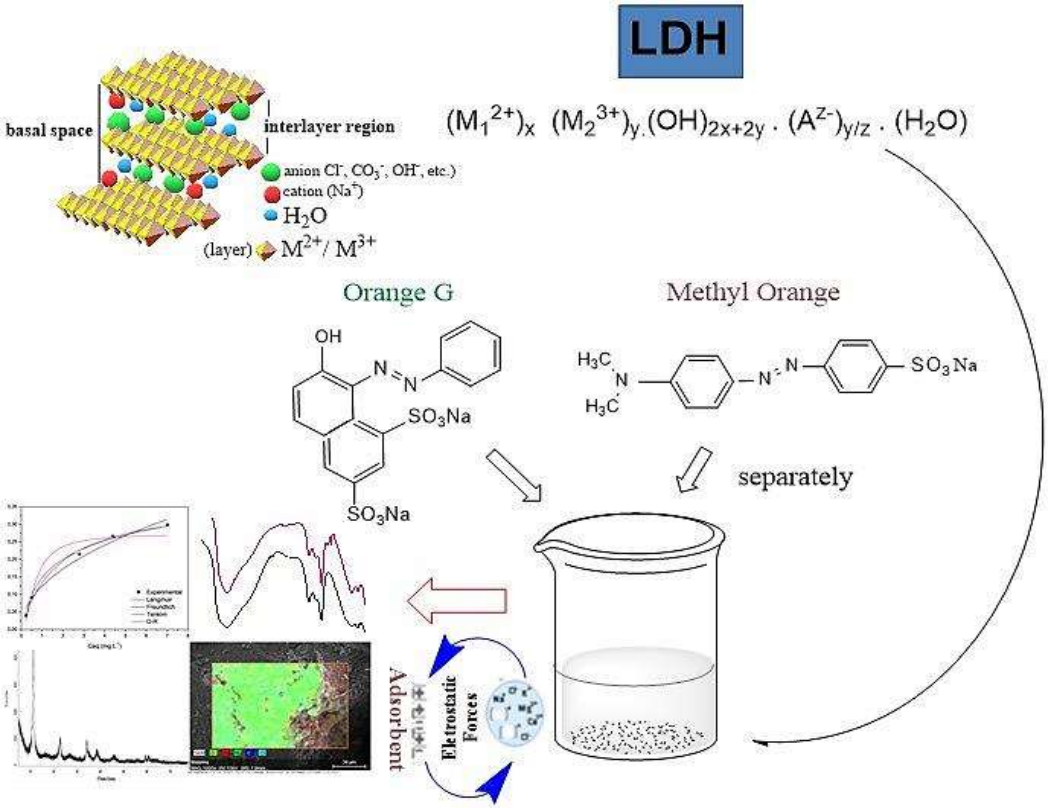

Title: Graphical Representation of the Adsorption of Anionic Dyes in MgFe HDL. Source: Author

Introduction

Anápolis and Jaraguá are the main industrial and logistics hubs in the Anápolis Microregion, which also includes important agro-industrial municipalities such as Inhumas and Itaberaí De Oliveira Junior et al. (2013). Industrial growth in urban conglomerates, coupled with a lack of public policies aimed at environmental protection, has had a negative impact on the quality of water resources Mohapi et al. (2020). One of the main factors associated with water degradation is the intensive use of synthetic dyes in various industrial segments, such as food, textiles, leather, paper, and pharmaceuticals Bentahar et al. (2018); Imgharn et al. (2022); Vo et al. (2025). The textile industry, in particular, is identified as one of the largest sources of contamination of water bodies, due to the high consumption of dyes and the improper disposal of effluents into the environment Jadham et al. (2023). Among these compounds, the azo dyes Orange G and Methyl Orange stand out, widely used in industrial processes and recognized for their high chemical stability and environmental persistence Danette et al. (2003); Vo et al. (2025).

The adsorption technique stands out among effluent treatment methods for its efficiency, operational simplicity, and low cost, and is widely used in the removal of organic and inorganic contaminants Murga et al. (2021). The choice of the appropriate adsorbent must consider factors such as waste composition, material cost, processing time, and interactions between the components of the solution. Several studies report the use of adsorbent materials, such as activated carbon Cunico et al. (2009), clays Chichinas et al. (2018); Sato et al. (2021), silicas Li et al. (2018); Maucec et al. (2017), double layer hydroxides (DLHs) Elmoubarki et al. (2017); Rios-

Leon et al. (2017); Mishra et al. (2018); Bukhtiyarova (2019), and chitosan and its derivatives Abbasi et al. (2016). These materials, applied alone or in hybrid matrices Tavares et al. (2014), allow for the adjustment of experimental conditions, increased efficiency, and the achievement of optimized systems to mitigate environmental contamination Laipan et al. (2019).

HDLs (Figure 1) stand out for their great compositional and structural versatility, as they can be formed by different combinations of divalent and trivalent cations, including Mg^{2+}, Zn^{2+}, Cu^{2+}, Fe^{3+}, and Al^{3+}. The layers of HDLs are positively charged and separated by anions, such as CO_3^{2-}, NO_3^-, SO_4^{2-}, PO_4^{3-}, in addition to water molecules, which ensures stability and flexibility to the structure Goh et al. (2008); Mahapatra et al. (2015). This lamellar organization allows the spacing between the layers and the surface area to be adjusted, directly influencing the adsorption and ion exchange properties Bukhtiyarova, (2019); Sato et al. (2021). It is worth mentioning that synthesis and post-synthesis treatments contribute to controlling the size, morphology, and uniformity of the particles, resulting in homogeneous structures with better performance Xu et al. (2006); Mohapi et al. (2020); and also that calcination transforms the structure into mixed oxides Ameena Shirin et al. (2021), with advantages Goh et al. (2008); and also disadvantages, as occurs in HDLs containing MgFe/CoCr Kang et al. (2020). Goh et al. (2008) mention that the production cost of HDLs, used as a porous vessel technique in the removal of pollutants, reaches US$ 0.12/day/20L to obtain drinking water. Due to these characteristics, HDLs have been widely studied as functional materials in contaminant removal processes.

In this context, the present study aimed to characterize the synthesized HDL Mg^{2+}/Fe^{3+} (MF41) and evaluate its efficiency as an adsorbent in the removal of the anionic dyes methyl orange and Orange G, widely used in industrial processes. The choice of HDL Mg^{2+}/Fe^{3+} is based on its environmentally friendly composition, formed by abundant metals with low toxicity and high chemical stability, which gives it a potential sustainable application in contaminated water treatment and remediation processes.

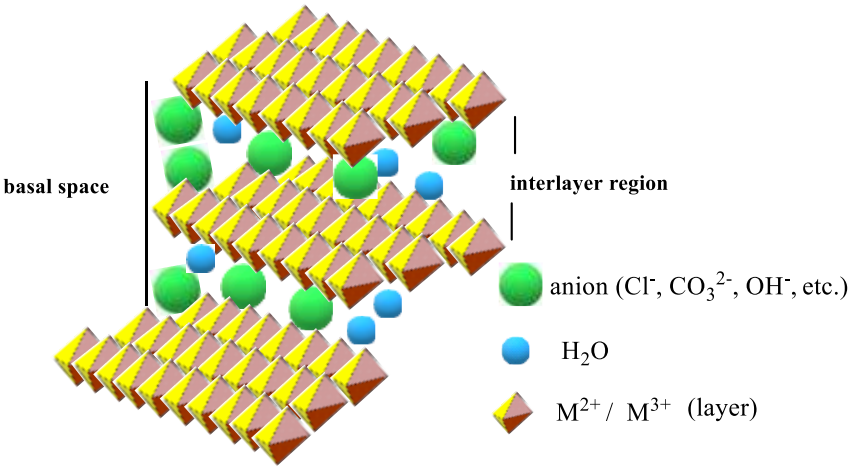

Figure 1- Representation of the HDL structure in organized lamellae. Source: Author

Materials and Methods

Materials

The orange dyes methyl orange (MO) (Figure 2a) and orange G (OG) (Figure 2b) dyes were purchased from Sigma-Aldrich (St. Louis, USA), hydrochloric acid (HCl), sodium hydroxide (NaOH), and all other compounds were obtained as analytical reagents from Sigma-Aldrich (St. Louis, USA).[

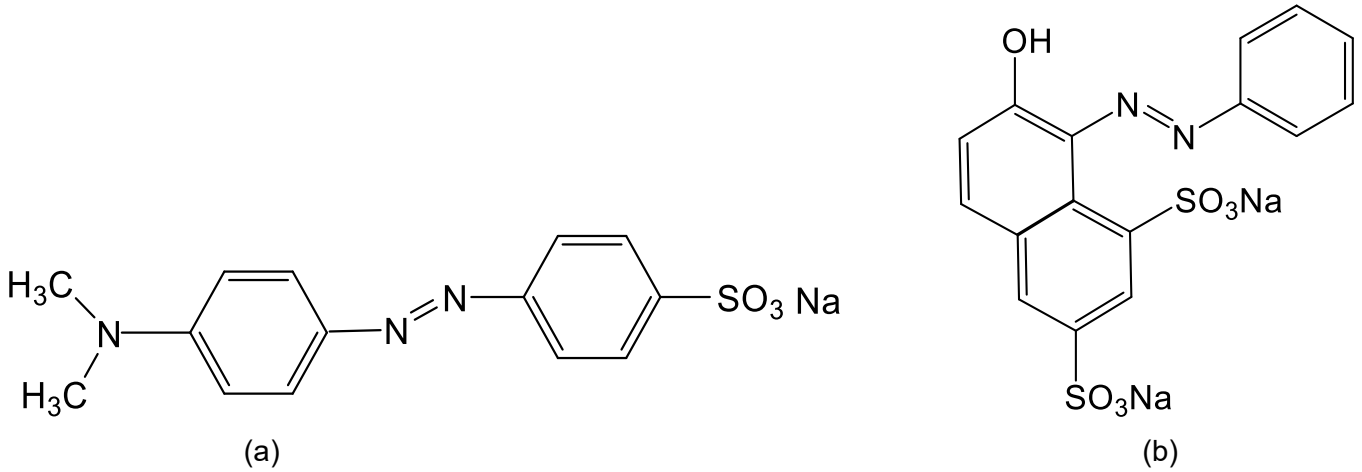

Figure 2- Azo dyes used: a) Methyl orange (MO); b) Orange G (OG). Source: Author

Methods

HDL synthesis

HDL was synthesized using the coprecipitation method. 100 mL of a solution of the metal salts M_1^{2+}($MgCl_2$) and M_2^{3+} ($FeCl_3$) salts in a flat-bottomed flask, molar ratio 4:1 (120 mmol of $MgCl_2$ / 30 mmol of $FeCl_3$), and an alkaline solution of NaOH (2.0 mol.L^{-1}) / Na_2CO_3 (0.2 mol.L^{-1}) was added by dripping at a rate of 1.0 mL/min, with constant and vigorous stirring at 700 to 800 rpm, until the pH of the solution reached 8.8 and stabilized. For hydrothermal treatment, a water condenser was attached to the assembly and the system was heated to 358K, kept thermally insulated by an external blanket, and subjected to constant stirring at 700 rpm for 24 hours. The system was then left to cool and decant for 2 hours. The precipitate was washed and filtered under reduced vacuum pressure until the washing water reached a pH of 6.25. The solid obtained was dried in an oven at 348K for 24 hours. After drying, the solid was manually ground in a porcelain mortar and pestle and separated into 40 to 150 mesh metal sieves. In a clean, dry environment, the solid was packaged in closed, labeled polyethylene bottles, separated by particle size, for the respective laboratory tests.

Structural Characterization

Characterization by Fourier transform infrared spectroscopy of the adsorbent before and after adsorption was performed using a PerkinElmer Frontier FTIR/NIR spectrophotometer (Waltham, USA) in the range of 400 to 4000 cm^{-1}using KBr (sample:KBr ratio of 1:100); and ultraviolet-visible (UV-Vis) spectroscopy was performed using a Metash UV-5800 Spectrophotometer, wavelength range 190 to 1100 nm, from Shanghai Metash Instruments Co. Ltd. (Shanghai, China). The morphology was analyzed by scanning electron microscopy (SEM/EDX) using Hitachi equipment (High-Tech Europe GmbH, Germany), model TM3030 Plus, with an electron acceleration voltage of 5kV to 15kV and an elemental composition analyzer (EDS); depositing portions of the samples on a carbon tape attached to an aluminum sphere. The analysis of the crystallinity patterns, symmetries, and structural behavior of the samples was performed using X-ray diffraction (XRD) on a Bruker D6 Phaser diffractometer, with a copper tube (λ = 1.54Å), in the angle range (2θ) from 5º to 80º (low initial angle), using continuous scanning at a speed of 0.05°min^{-1} , and the voltage used was 40 kV with currents of 30 mA / 15 mA. The thermogravimetric analyses of the samples were obtained using a P1TGA (Perkim Elmer) instrument employing a dynamic atmosphere of N_2 at a flow rate of 20 mL min^{-1} , with a heating ramp at a rate of 10 ºC min^{-1} , starting at 25 ºC up to a temperature of 700 º C.

Particle Size Suitability.

For the particle size suitability test, 20 mg samples of MF41 solid were separated into different sizes (40, 60, 80, 100, and 150 mesh) and dispersed in 50 mL of dye solution (10 mg L^{-1}). The adsorption kinetics were performed in duplicate, and the most suitable particle size was 100 mesh in all adsorption kinetics, pHPCZ, and particle dispersion.

Network Parameters and Calculation Method

To confirm the phases, the diffraction peaks (2θ) were analyzed to determine the particle size of the synthesized material using the Scherrer formula (d= 0.9λ / fwhm cos θ), where: d is the crystallite size (nm), λ is the wavelength of the monochromatic X-ray beam (nm), (λ is 0.154056 nm for CuKα radiation), fwhm is the "full width at half maximum" for the diffraction peak under consideration (rad), and θ is the Bragg angle (degrees) Banerjee et al. (2019).

Adsorption Studies

pH Study $_{PCZ}$

To determine the zero charge point (pH_{PCZ}), 20 mL of 0.1 mol L^{-1}NaCl solution at different pH values (2-12) in triplicate were added to 20 mg of the adsorbent and corrected to the desired pH using NaOH and/or HCl solution (0.1 mol L^{-1}). The samples were stirred at 100 rpm for 24 h at 298 K. Afterwards, the solutions were filtered and the final pH was measured. To determine the pH_{PCZ}, a graph of the final pH as a function of the initial pH was constructed. The $pH_{PCZ}$is the point at which the difference between the final pH and the initial pH is zero, behaving like a buffer solution Liu et al. (2006b); Komulski, M. (2009) (2018).

Equilibrium and Chemical Kinetics

The dye concentrations before and after equilibrium were determined using a Metash UV-5800 Spectrophotometer at a wavelength of 465 nm for MO and 478 nm for OG. The adsorption studies were performed in triplicate. The percentage dye removal and adsorption capacity (q_e) were calculated according to Equations 1 and 2, respectively:

$$remoção\ (\%)\ C_0 = \frac{C_0 - C_{eq}}{C_0} x\ 100 \qquad (1)$$

$$q_e = \frac{(C_0 - C_{eq})\ x\ V}{m} \qquad (2)$$

Where: $C_0$and C_{eq}:are the concentrations (mg $^{L^{-1}}$) of the dye in the aqueous phase at the initial concentration (C_0) and after equilibrium (C_{eq}), respectively; q_e : the equilibrium adsorption capacity (mg $^{g^{-1}}$), m: the mass of the adsorbent (g), and V: the volume of the solution (L) Murga et al. (2021).

For the chemical adsorption kinetics studies, 100 mg of adsorbent, with a particle size of 100 mesh, was added to 50 mL of dye solution at a concentration of 10 mg $^{L^{-1}}$. The suspensions were kept under stirring (100 rpm) for 24 h at 298 K. HCl and NaOH solutions (0.1 mol $^{L^{-1}}$) were used to adjust the initial pH to the optimum pH of 8.05. The kinetics were studied using the pseudo-first-order (Equation 3), pseudo-second-order (Equations 4 and 5), and intraparticle diffusion (Equation 6) models. The relationship between the amount of adsorbates retained in the adsorbent per unit mass and the concentration of the adsorbate in solution at

equilibrium, at a given temperature, allowed us to ascertain the affinity, behavior, characteristics, and conformity of the adsorption sites according to Giles et al. (1974); Elmoubarki et al. (2017); Murga et al. (2021).

$$\log(q_e - q_t) = \log q_e - \frac{k_1}{2{,}303} \times t \qquad (3)$$

$$\frac{1}{qt} = \frac{1}{V_o} + \frac{1}{q_e} \times t \qquad (4)$$

$$V_o = k_2 \times (q_e)^2 \qquad (5)$$

$$q_t = k_d \times (t)^{1/2} \qquad (6)$$

Where: parameters q_e : concentration of dye adsorbed by the adsorbent, q_t: amount of dye adsorbed at time t, k_1 and k_2 : first-order and second-order rate constants, respectively, t: time in the adsorption process, V_0: pseudo-second-order reaction rate, and k_d: diffusion rate constant in accordance with Bentahar et al. (2017); Zhang and Liu et al. (2017); Konick et al. (2018).

Study of the Effect of Particle Dispersion

Samples of 10 mg of MF41 adsorbent, before and after adsorption with the dyes, were dried at 90°C in an oven and then dispersed in 10 mL of deionized water. The test tubes containing the samples were identified and separated. The samples were homogenized in a vortex for 3 to 5 minutes and left to stand for 24 hours. Under these conditions, visual observations of the samples were made over time (5, 10, 15, 20, 30, 40, 60, 80, 100, 1380, and 1440 min) to identify the dispersed phase (particles) and the dispersing phase. The images from the visual examinations (Appendix A) provided data to identify the degree of particle dispersion, as follows: A – MF41, B_1 - MF41 with OG (10 mgL^{-1}), B_2 - .MF41 with OG (20 mgL^{-1}), C - . MF41 with MO (10 mgL^{-1}).

Data Normalization and Treatment

Data normalization was performed to ensure logical consistency and eliminate redundancies. Each parameter analyzed (transmittance, absorbance, count, intensity, etc.) was scaled in the range from 0 to 1, preserving the proportions and distribution of the original data.

Results and Discussion

Characterization

The spectrum of HDL MF41 (Figure 3) indicates the presence of an absorption band at 1640 cm^{-1} to 1590 cm^{-1} corresponding to water deformation - $\delta(H_2O)$; and a characteristic band at 1380 cm^{-1} related to v_3 (asymmetric stretching) of the CO_3^{2-} ion in the intermediate layer, intralamellar region of HDL Bukhtiyarova (2019); Kang et al. (2020); Jadham et al. (2023). A typical elongated band of MF41 material appears at 1200 cm^{-1} Elmoubarki et al. (2017). However, the bands in the low-frequency region (below 1000 cm^{-1}, except for carbonate) are related to the metal-oxygen and metal-oxygen-metal vibrational modes in the layer, similar t , the brucite-type mineral Rios-Leon et al. (2017); Kang et al. (2020). Characteristic stretching and out-of-plane deformation bands related to ions (CO_3^{2-}) are present at 690 cm^{-1} to 670 cm^{-1} (Table 1).

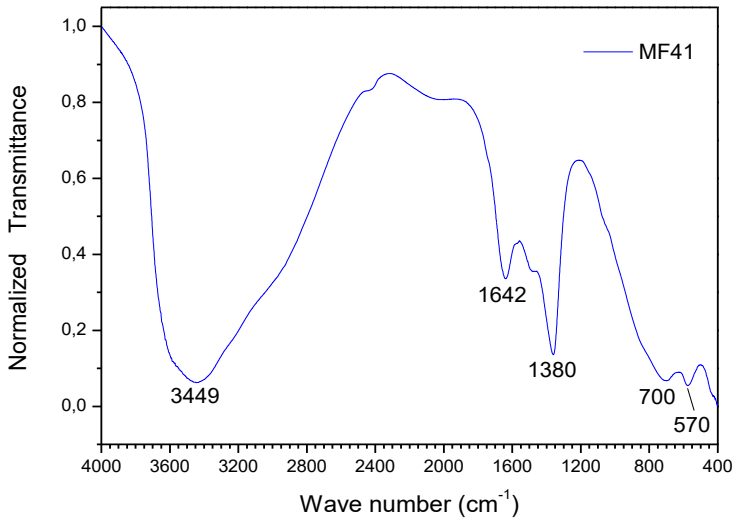

Figure 3 - MF41 FT-IR spectrum. Source: Author

As described in Table 1, the MF41 spectrum with MO (Figure 4a) showed an absorption band at **1232** cm^{-1} characteristic of the C-N bond, typical of the presence of aliphatic and aromatic amines; and a narrow band at **1153** cm^{-1} characteristic of the asymmetric stretching of the adsorption of R-SO_3^- species in the solid Leont`Eva et al. (2022); Kong et al. (2023); Liangquan et al. (2024). The MF41 spectrum with OG (Figure 4b) showed a band at **1168** cm^{-1}, an asymmetric stretching characteristic of the adsorption of R-SO_3^- species in HDL.

Table 1. Stretching frequency values before and after adsorption.

Assigment	**MF41** (cm^{-1})	**MF41 + MO** (cm^{-1})	**MF41 + OG** (cm^{-1})
VOH	3449	3449	3449
δH_2O	1642	1641	1634
$V_3CO_3^{2-}$	1380	1368	1368
δ C-N	-	1232	-
R-SO_3^-	-	1153	1168
$V4CO_3^2$	700	693	699
VM-O-M	570	568	576

Source: Author

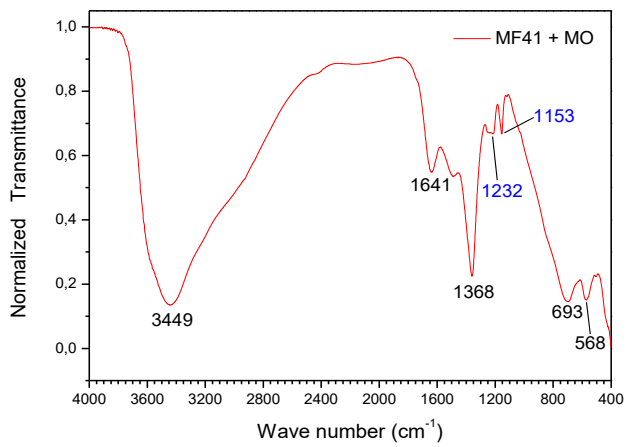

a) FT-IR spectrum MF41 with MO;

(a)

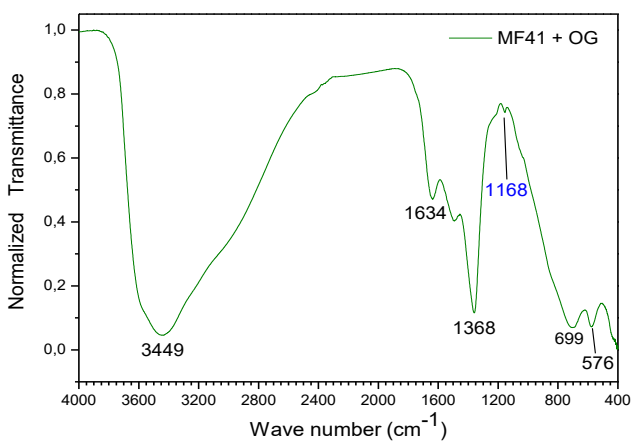

b) FT-IR spectrum MF41 with OG. Source: Author

(b)

The textural and morphological properties of the MF41 sample at different magnifications, shown in scanning electron microscopy (Figure 5), presented a rough and irregularly shaped surface with spaces between the particles, forming a hierarchical structure of grains in the form of stacked plates or overlapping plates Nguyen-Thanh et al. (2005); Tichit et al. (2024) which increases the contact area as mentioned by Kong and researchers (2023).

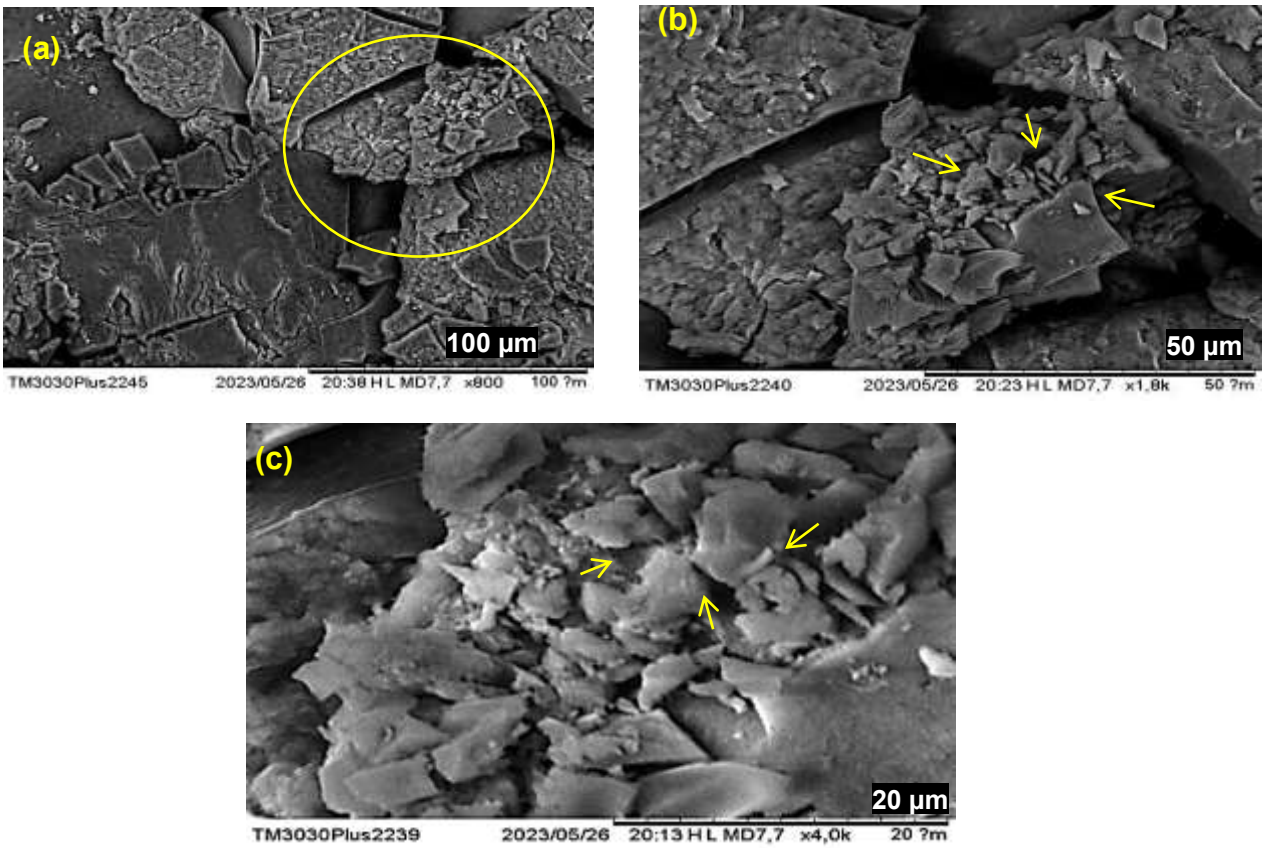

Figure 5 - Scanning electron micrographs of the adsorbent: (a) 800x, (b) 1800x, and (c) 4000x. Source: Author

One of the main advantages of heat treatment in synthesis is the formation of an organized crystalline structure due to hydrothermal treatment and aging time. This procedure improves the shape of the particles (crystallites), contributes to the purity and increases the surface area of the material, minimizing the formation of unwanted interferents. Soliman & Aly (2019); Ameena Shirin et al (2021). It was observed that the hydrothermal treatment used for the material was effective, given the structural organization achieved and the purity of MF41. The micrograph analyses with EDS of MF 41 (Appendix B), the element map (Appendix B), and the composition map (Figure 6) reveal the presence of Mg^{2+}/ Fe^{3+}ions in the MF41 adsorbent sample before adsorption.

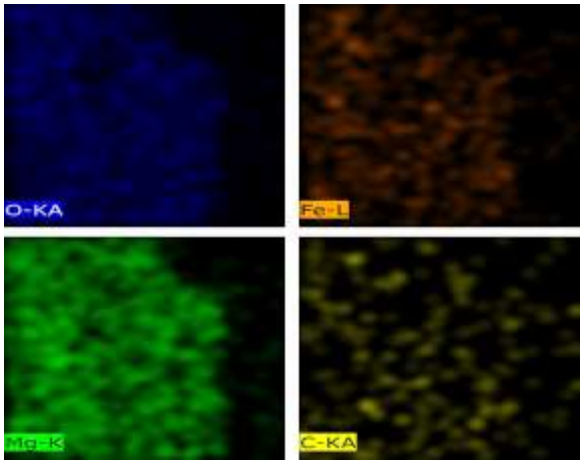

Figure 6 - Composition map of MF41. Source: Author

Figures 7 and 9 show the EDS micrographs and element maps of MF41 with OG (Figure 8) and MO (Figure 10) dyes. The analyses indicate the existence of chemical species not present in the initial composition of the material. The chemical species inherent to the sulfur (S) element is not part of the compounds used in the original synthesis. It is suggested that the significant amount of sodium (Na) found in the micrographs (Figures 7 and 9) also originates from the dye adsorption process.

Figure 7 - Micrograph with EDS of MF41 with OG - 600X. Source: Author

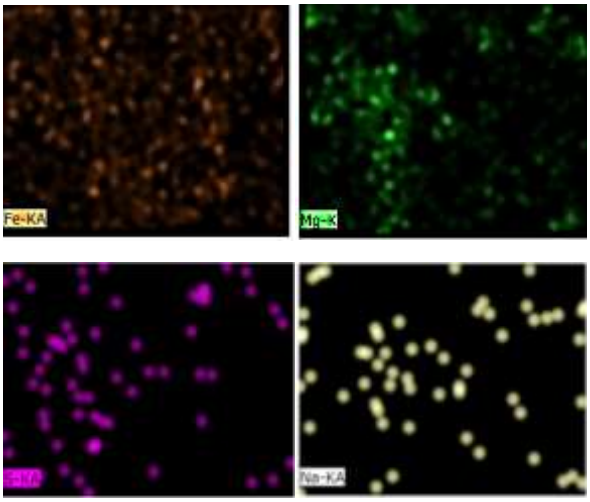

Figure 8 - Element map of MF41 with OG. Source: Author

Figure 9 - EDS micrograph of MF41 with MO - 400X. Source: Author

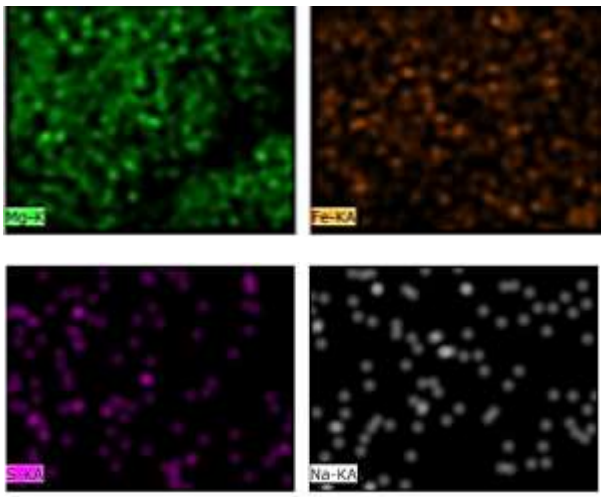

Figure 10. Element map of MF41 with MO. Source: Author

Note: the carbon present in the samples (Figures 7 and 9) is related to the carbon tape used to fix the samples in the analysis method.

The crystallinity and absence of interferents denoting phase transitions (Figure 11), indexed by the peaks (2θ) at: (003), (006), (012), (015), (110), and (113), are in accordance with the typical diffraction patterns of HDL solids presented by Duan & Evans (2006); Das et al. (2006) and reports described by researchers such as Goh et al. (2008); Trujillo et al. (2016); Bukhtiyarova (2019); Kong et al. (2023).

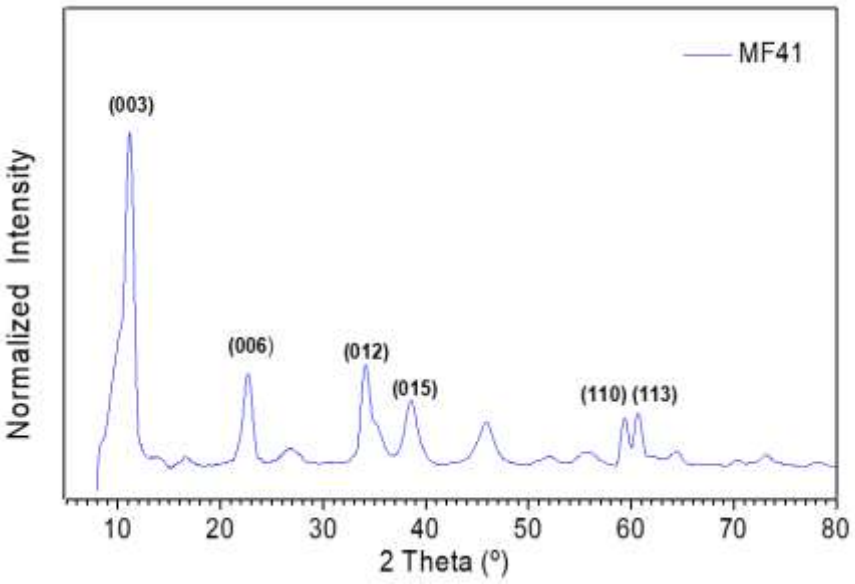

¶

Figure 11 - X-ray diffractogram of MF41. Source: Author

The crystallization of the respective solid occurred in the ordered form of cations as described by Manohara et al. (2011) because the peaks indexed at (2θ) do not denote phase transitions, nor any additional unidentified reflections between peaks (003) and (006) belonging to the interlayered phase, due to stacking faults and/or phase coexistence Bukhtiyarova et al. (2019); Leont'eva et al. (2022). Furthermore, no $Mg(OH)_2$chemical species was observed in the XRD of MF41 (Figure 11), which could result in a poorly crystalline structure and/or affected by the buffer effect during co-precipitation Bukhtiyarova et al. (2019); with nucleation occurring at short time intervals Manohara et al. (2011) similar to the mineral brucite Khan et al. (2009); Leon et al (2017).

The ordered form and non-coexistence of HDL phases indicate that the intercalated anions do not contain atoms with high scattering power, and the intensities of the basal reflections (00l) are mainly governed by the intensity of the X-rays scattered by the metal cations in the host layers. Therefore, the intensities (00l) decrease as l increases, and the reflections (00l) are well defined. Thus, there is a one-dimensional distribution of electron density along the c axis in HDL Duan & Evans (2006); Bukhtiyarova et al. (2019).

In particular, the evolution of the angular position of the 00l reflection highlights the possible intercalation of organic species, while the presence of additional patterns may indicate possible crystallization on an external surface or a reorganization of the structural phase Sato et al. (2021). Zhang et al. (2019) mention that the high concentration of a surfactant salt promotes an effect on X-ray diffraction between the (003) and (006) peaks, and can be easily observed through the appearance of a characteristic peak, in an enlarged peak, close to 20º (2θ), representative of the intercalation of the organic compound in HDL, as an intercalating anion Duan & Evans (2006). However, low concentrations of a dye can be identified in XRD, accompanying any changes in the reflections of (00l) if the charge of the organic species is sufficient to destabilize the lamellae, which causes variations in the peaks (2θ) at low angles Sato et al. (2021)

In this circumstance, the existence of the characteristic broad peak at 17.95º (2θ), observed in the MF41 diffractogram with MO (Figure 12), between the diffraction planes $d_{(003)}$and $d_{(006)}$ Duan & Evans (2006);

Zhang et al. (2019); added to the broad absorption band of the functional groups (C-N) at 1240 cm^{-1} , and the narrow and apparent absorption band at 1153 cm^{-1} (Fig. 4a) related to functional groups of the type [R-SO_3^-] in the infrared spectrum, indicate the intercalation of the dye in the HDL structure.

In Table 2, the adsorption of OG in HDL indicates an increase in the basal spacing associated with the lattice parameter $d_{(003)}$ with the broadening of the peak indexed at 10º (2Θ) (Figure 12). There was an electrostatic destabilization of the structures in the stacking of lamellae in HDL as mentioned by Zhang et al. (2019), and this was governed by the decrease in electrostatic interaction between positive and negative lamellae Duan & Evans (2006); Leon et al. (2017); Sato et al. (2021). Therefore, the slightly pronounced peaks at (2Θ): (a) 20.54º and (b) 26.50º, recorded in the diffractogram (XRD) (Figure 12) of MF41 with OG, added to the weak signal in the infrared spectrum at 1168 cm^{-1} (Figure 4b), indicate the adsorption of the dye in HDL.

Table 2. Network parameters of the samples.

Sample	d $_{(003)}$ Å	d $_{(006)}$ Å	d $_{(110)}$ Å	C= 3d $_{(003)}$ Å
MF41	7,9249	3,9392	1,5572	23,77
MF41 c/ MO	7,8126	3,8929	1,5484	23,43
MF41 c/ OG	8,5093	3,9274	1,5535	25,94

Source: Author

The scenario suggests that adsorption is associated with the electrostatic effect of hydrophilic sulfonate groups (SO_3^-) in OG Das et al. (2006); Sato et al. (2021). These negatively charged groups promoted internal instability and expansion of the interlayer space in HDL Sato et al. (2021), observed by the broadening of the peak indexed at (2Θ) by 10º and by the increase in the absolute value of the network parameter d(003) Zhang et al. (2019); Sato et al. (2021).

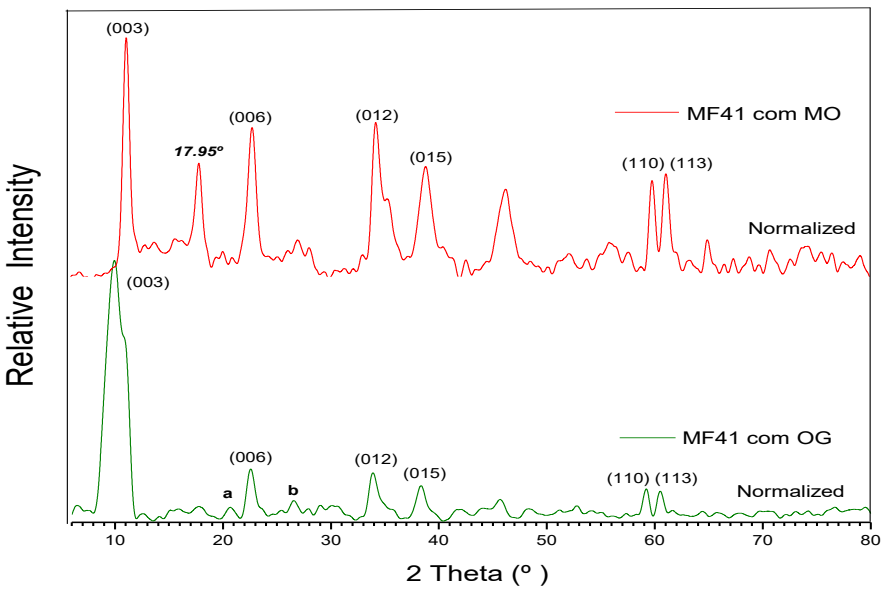

Figure 12 - X-ray diffractograms of MF41 with dyes. Source: Author

The variation in mass in relation to temperature, thermogravimetric events, and system properties allowed us to determine the temperature range in which the samples acquired a fixed chemical composition. Thus,

understanding the phenomena of dehydration, metal oxidation, and decomposition made it possible to understand the thermogravimetric behavior of the solid before and after adsorption.

Mass loss due to interlamellar water removal and lamellar dehydroxylation occurred from 25 °C to 180 °C for the MF41 adsorbent (Figure 13a) Luengo et al. (2017); Rios-Leon et al. (2017); Bukhtiyarova (2019). However, the same losses for MF41 with MO (Figure 13b) occurred from 120 °C to 280 °C, indicating that the dye molecules occupied the interlamellar water spaces in the solid. Therefore, a lower amount of water and/or OH- ions in the second stage of decomposition is justified, reflecting a higher percentage of mass loss at higher temperatures (Table 3) Elmoubarki et al. (2017); Rosset et al. (2022).

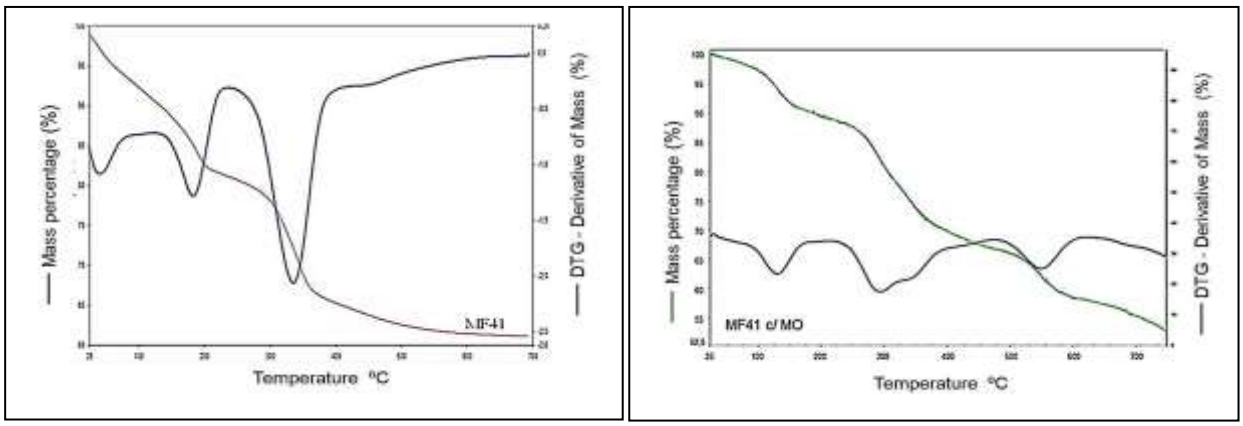

Figure 13 - a) Thermogravimetric analysis of MF41; b) Thermogravimetric analysis of MF41 with MO.

(a) **(b)**

Source: Author

In this context, the mass loss that occurred between 280 °C and 380 °C in MF41 with MO (Figure 13b) is related to the decomposition of the HDL structure with the formation of metal oxides and the onset of decomposition of carbonate anions in the structure. In addition, the marked mass loss from 380 °C to 550 °C (Figure 13b) indicates that there was a greater amount of carbonate ions bound to chemical species of the dye in the interlayer region. This promoted an increase in the final decomposition temperature of η-CO_3^{2-}(carbonate) ions and reflected a high percentage of mass loss at this stage of heating (Table 3) Rios-Leon et al. (2017); Rosset et al. (2022) when compared to MF 41 and MF41 with OG.

Table 3. Percentage of mass loss due to temperature before and after adsorption.

Sample	1st Stage (25º to 120 ºC) [H_2O / OH^-]	2nd Stage (120º to 200 ºC) [H_2O residual /OH^-]	3rd and 4th Stages (220º to 380 ºC) [R-MO^{2-} / R-CO_3^2]	5th Stage (above 380 ºC) [decomposition ηCO_3^{2-}]
MF41	8,52 %	8,98%	16,67 %	5,53%
MF41 + MO	7,50%	4,50%	18,00%	17,37%
MF41 + OG	6,25%	8,75%	17,50%	6,70%

Source: Author

The MF41 sample with OG (Figure 14) and the MF 41 sample (Table 3) show very similar percentages of mass loss. This indicates a low amount of dye adsorbed in the solid.

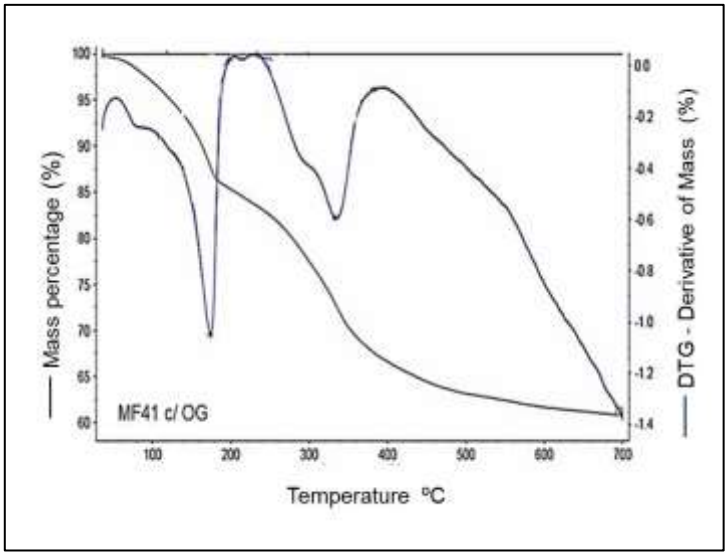

Figure 14 - Thermogravimetric analysis of MF41 with OG. Source: Author

Adsorption Studies

pH_{PCZ}

Based on the relationship between the initial pH and the final pH of the solution, the pH_{PCZ} of MF 41 was calculated using the arithmetic mean of the points, in triplicate, whose final pH is constant, functioning as a buffer solution (Figure 15). The value found for the pH_{PCZ}parameter of the adsorbent was 7.45 ± 0.03, similar to values reported in the literature as described in Table 4. Analysis of the pH_{PCZ}associated with the MF41 structure suggests that if the pH of the solution is lower than the pH_{PCZ}($pH_{solution}$< 7.45), the surface of the adsorbent will be positively charged, increasing and favoring the adsorption of negatively charged dyes through electrostatic forces Elmoubarki et al. (2017); Hao et al. (2018); Murga et al. (2021).

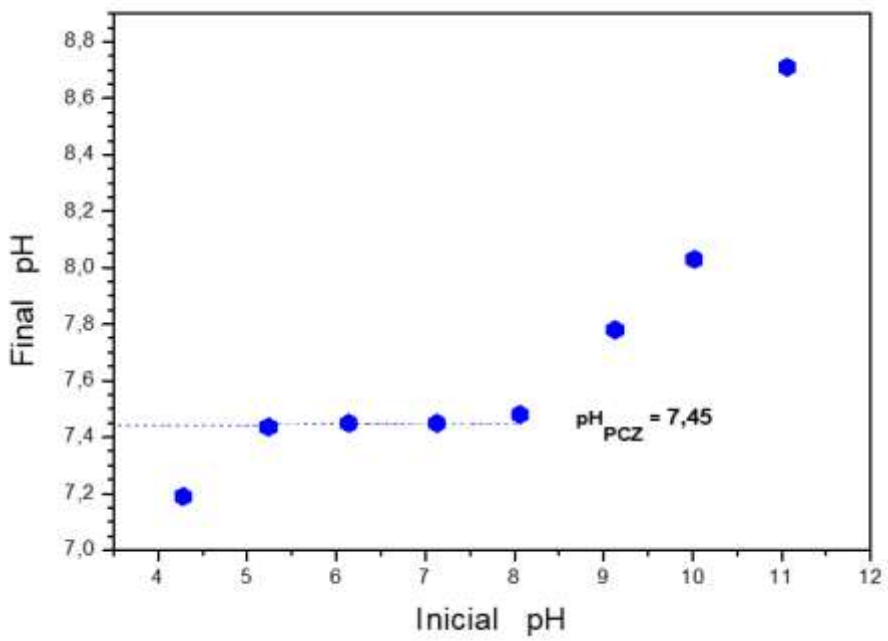

Figure 15 - Graph of the zero charge point of the adsorbent.. Source: Author

Table 4 shows values of different HDLs found in the literature compared to the $pH_{PZC}$of the adsorbent sample.

Table 4. Comparison of the pH_{PZC} obtained in this study with values reported in the literature.

Material	pH_{PZC}	Reference
Uncalcined chloride Li–Al LDHs	7.2	Liu et al. (2006)
Uncalcined chloride Zn–Al–Fe LDHs	9.3-10.0	Jiao and Hou (2007)
γ-FeOOH	7.4	Jiao and Hou (2007)
Magnetic HDL-Mg/Al	8.1	Eftting et al. (2017)
HDL- CaAl – RE	12.15	Henrique et al. (2023)
Uncalcined Mg–Fe LDHs	8.7 / 8.9	Goh et al. (2008)
CG1 / CG2 (AAH)	6.50 / 7.62	Scholtz et al. (1985)
MF41	7.45	This work

Source: Author

It should be noted that three modes can govern the adsorption mechanisms in HDLs, such as: electrostatic attractions, anionic exchange, and surface complexation mentioned by Luengo et al. (2017). Considering that the pH of the solution directly affects the surface charge of the material and the degree of ionization of the adsorbates Brião et al. (2017); Alves et al. (2025), it is necessary to consider two factors that can influence the adsorption process and its mechanisms, such as: the protonation state of the dyes and the behavior of the charges on the surface of the adsorbent.

Since the dissociation constant (pKa) of MO in aqueous solutions has values close to 3.46 (Alves et al., 2025), and the sulfonate groups of MO (SO_3Na) are dissociated and are in anionic form, predominating at pH values higher than pK_a(Pei et al., 2007). Considering that the removal percentage (Figure 17a) and adsorption capacity (q_e) of MO in the solid described in Table 6 were higher at pH 8.0 than at pH 6.0 (Appendix B), it is suggested that intermolecular interactions were governed by electrostatic forces between the sulfonate groups

($^{SO_3^-}$) of the dye and the available adsorption sites in the solid Pei et al. (2007). Mallakpour and Motirasoul (2021) mention that ΔG° values between −20 kJ and 0 kJ mol^−1indicate physical adsorption, and between −80 kJ and −400 kJ mol^−1indicate chemical adsorption. The ΔG° values of – 17.10 kJ $^{mol^{-1}}$ for MF41 with MO at pH 8.0 and – 16.69 kJ $^{mol^{-1}}$ at pH 6.0 (Appendix C) indicate that the nature of the adsorption is physical and that electrostatic interactions, hydrogen bonds, and/or dipole-dipole forces governed the adsorption of MO molecules on the solid Pei et al. (2007); Mallakpour and Motirasoul (2021).

OG, in aqueous solution, has a pK_avalue of 11.5 ± 0.02 for the hydroxyl hydrogen in the aromatic ring Cai et al. (2016); Haddou et al. (2011), and a $pK_a$of 1.0 for the two SO_3 H groups (Cai et al. (2016). As the solution has a pH of 8.0, the OG dye is in its anionic form Madhavan et al. (2010), and the sulfonate groups (SO_3^-) govern the electrostatic interactions between the dye and the surface of the lamellar solid Cai et al. (2016). Adsorption in HDL suggests functionalization of the solid through lamellar intercalation of the dye.

Goh et al. (2008) mention that there is a combined chemical and electrostatic effect that promotes adsorption on uncalcined HDLs when pH > pH_{PCZ}. Sato et al. (2021) mention that there is an electrostatic effect associated with the charges present in the polar region of the adsorbate. This effect promotes dye intercalation in the HDL structure in the same way as occurs with anionic surfactants Sato et al. (2021).

Adsorption Equilibrium and Kinetics

The adsorption kinetics were investigated to establish the ideal contact time between the adsorbent (MF41) and the adsorbates (dyes) when equilibrium is reached by the system (Almeida et al., 2009). In the experiment, the temperature was maintained at 298K, and the system parameters (particle size, temperature, system pH, and solution volume) were kept constant. The equilibrium and concentration coefficients (q_e) of adsorption were calculated according to the contact time Sheng et al. (2018) at the respective temperature.

It was observed that equilibrium occurred around 210 minutes for MF41 with MO and 150 minutes with OG. The maximum removal percentage was 70% and 87.5%, respectively, for MF41 with MO (Figure 16a) and MF41 with OG (Figure 16b). At a pH of 6.0, the equilibrium time for MF41 with MO occurred in 200 minutes, and the maximum removal percentage reached 64.9% in 150 minutes (Appendix B).

A sharp increase in removal was observed in the first 60 to 80 minutes. After that, the systems showed a lower rate of change until reaching maximum removal and kinetic equilibrium at around 150 minutes (Figures 16a and 16b). The initial rate of filling of the active sites in the adsorbent was high, followed by a slower reaction over time until the systems reached equilibrium, suggesting an L-type isotherm Gilles et al. (1974); Elmoubarki et al. (2017). This occurred due to the decreasing number of active adsorption sites available, due to the progressive coverage of the adsorbent surface Banerjee et al. (2019).

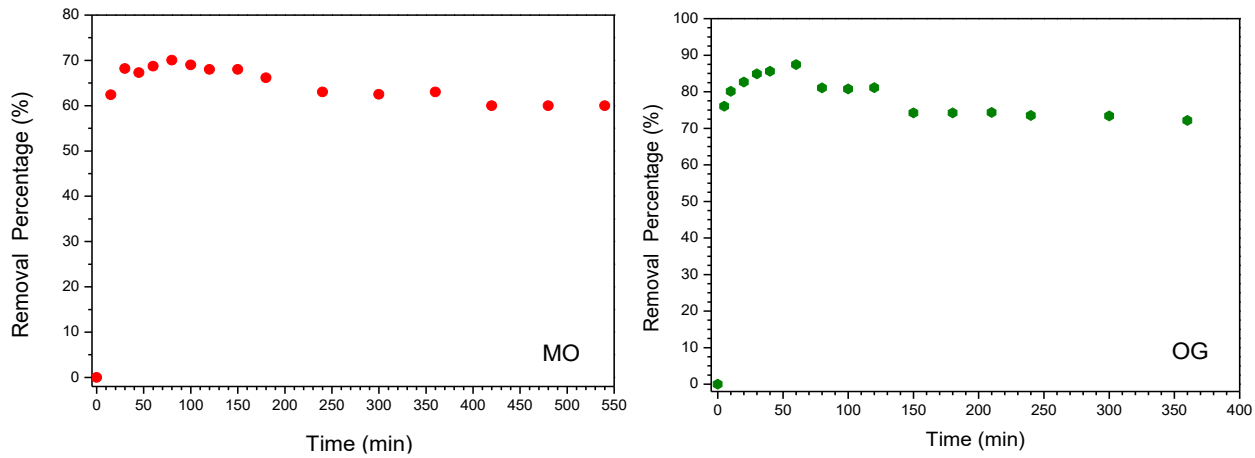

Figure 16 - a) Removal of MF41 with MO; b) Removal of MF41 with OG. Source: Author

(a) **(b)**

Of the kinetic models constructed, the model that best described the adsorption of MO and OG dyes (Table 5) was the pseudo-second order model, with coefficients close to 1 (one). Some studies involving the application of models to explain the adsorption kinetics in HDL and its derivatives, reported in the literature, provide correlations with the pseudo-second-order model De Sá et al. (2021); Henrique et al. (2022); Kausar et al. (2018).

Table 5. Adjustments for kinetic models of dye adsorption on the adsorbent.

Dye	Type of adjustment	1st order	2nd order	Interparticle Diffusion
MO	R squared	- 0.0323	0.9916	0.8458
	Pearson`s	- 0.1795	0.9960	0.9252
OG	R squared	0.2731	0.9970	0.3131
	Pearson's	-0.0794	0.9990	0.6053

Source: Author

Table 6 shows the physicochemical parameters obtained in the kinetic study of the dyes, such as: the rate constants (K_1 and K_2) in the pseudo first-order and second-order models, the experimental results, and the adsorption capacity.

Table 6. Physicochemical parameters of adsorption kinetics.

System	V_0	K_1	K_2	$q_{e\ máx}$
MF41 + MO	2.39×10^{-2}	2.92×10^{-4}	1.85×10^{-3}	3,7109
MF41 + OG	1.42×10^{-2}	2.77×10^{-6}	7.93×10^{-4}	4,2328

Source: Author

Effect of Particle Dispersion

The study sought to identify the presence of dyes in the solid, as well as to understand the stability of the system (adsorbent-adsorbate) and the behavior of the electrostatic forces present when it is subjected t e solvation. The solid acts as a matrix that retains the dyes through intermolecular forces and, when solvated, becomes passive to the electrostatic forces promoted by the solvation phenomenon. Similarly, studies on solvation in zeolites and nanomaterials indicate that the behavior of solvation is complex, and the factors that control solvation depend on the reaction kinetics, the type of solvent, the type of solid, and its surface Zhou & Xu (2018); Chen and Getman (2024); Mapile et al. (2024).

The visual analyses presented in Appendix A indicated that sample C (MF41 in the presence of MO) presented a greater state of dispersion and a lower tendency to aggregate, evidencing a more stable suspension compared to the other conditions evaluated. The MF41–MO suspension showed initial stability due to electrostatic interactions between HDL Mg/Fe and the sulfonic groups of the dye, associated with the solvation of the particles and the hydrophobic character of the aromatic portion of the dye, which contributes to hindering the approximation and aggregation between the dispersed particles Mapile et al. (2024). Together, these factors inhibit immediate aggregation and maintain the system dispersed in the initial stages. However, as the sedimentation process began to dominate over the stabilizing forces, slow and progressive particle deposition was observed.

In turn, samples B1 and B2 (MF41 in the presence of OG at 10 mg L^{-1} and 20 mg L^{-1}, respectively) showed low colloidal stability, evidenced by rapid aggregation and sedimentation of the material, without causing significant interference in light diffraction by the medium. This behavior suggests that, under these conditions, the system did not maintain sufficient repulsive force or solvation to sustain the particulate dispersion Mapile et al. (2024), which resulted in the almost immediate deposition of the particles. However, a detailed interpretation of the mechanism, including the extent of adsorption or the nature of the interactions in the adsorbent-adsorbate complex, requires complementary instrumental analyses in addition to the visual test employed.

Conclusion

Under the conditions studied, the positive adsorption results demonstrated that the material has an affinity for anionic dyes. Hydrothermal treatment improved the size and shape of the particles, minimizing the formation of unwanted interferents. The rough and irregular surface, with interparticle voids, provided a larger contact area between the HDL and the dyes. X-ray diffraction and thermogravimetric analyses indicate that the orange methyl dye is adsorbed on the solid. The adsorption kinetics of MF41 with MO showed a better removal percentage at pH 8.0 than at pH 6.0, indicating that intermolecular interactions occurred between the sulfonate group (SO_3^-) in the dye and the available adsorption sites in the solid. The adsorption of OG on HDL suggests an adsorption model similar to that which occurs in a surfactant salt. The increase in the basal spacing in $d_{(003)}$ for MF41 with OG, the characteristic peak near 20º (2θ) in the XRD of MF41 with MO, associated with a higher percentage of removal at a pH higher than pH_{PCZ} and the $\Delta G°$ values found for the systems, indicate that adsorption in HDL was governed by a combined chemical and electrostatic effect, with the latter being predominant. The results obtained reinforce the potential use of Mg/Fe HDLs in sustainable applications in the remediation and/or final polishing of contaminated water, due to their environmentally friendly composition, formed by abundant metals, low toxicity, and high chemical stability.

Acknowledgments

The authors would like to thank the State University of Goiás (UEG), the Federal Institute of Goiás (Goiânia Campus), and CAITEC (UEG Center for Analysis, Innovation, and Technology) for their technological support; and the State University of Goiás for its financial support ( ): Pro-programs 2023 and 2024 (processes SEI 202300020011096 and 202400020010903) and pro-projects 22/2022 (SEI: 202200020022909).

References

Abbasi M, Habibi MM. 2016. Optimization and characterization of direct Blue71 removal using nanocomposite of chitosan-WCNTs: Central composite design modeling. J. of Institute Chemical Engineers (62): 112-121. https://doi.org/10.1016/j.jtice.2016.01.019

Almeida CAP, Debacher NA, Downs AJ, Cottet L, Melo, CAD. 2009. Removal of methylene blue from colored effluents by absorption on montmorillonite clay. J. Colloid Interface (332): 46-53. https:// doi:10.1016/j.jcis.2008.12.012

Alves RT, Terceiro PS, De Araújo CB, Ribeiro AS, Pereira MSS, Da Cunha AR, De Oliveira IN, Manzoni V. 2025. Solvatochromic effects on anionic and protonated forms of methyl orange dye: An experimental and

theoretical study. Spectrochimica Acta Part A: Mol. and Biomolecular Spectroscopy (343):126530. https://doi.org/10.1016/j.saa.2025.126530

Ameena Shirin VK, Sankar R, Jonhson AP, Gangadharappa HV, Pramod K. 2021. Advanced drug delivery applications of layered double hydroxide. J. Controlled Release 330 (2021) 398–426. https://doi.org/10.1016/j.jconrel.2020.12.041

Banerjee S, Dubey S, Kumar Gautam R, Chattopadhyaya MC, Sharma YC, 2019. Adsorption characteristics of alumina nanoparticles for the removal of hazardous dye, Orange G from aqueous solutions, Arabian J. of Chemistry (12) 8: 5339-5354. https://doi.org/10.1016/j.arabjc.2016.12.016.

Bentahar S, Dbik A, Khomri M, Messaoudi N, Lacherai A. 2017. Adsorption of methylene blue, crystal violet, and Congo red from binary and ternary systems with natural clay: Kinetic, isotherm, and thermodynamic. J. of Environmental Chemical Engineering (5): 5921-5932. https://doi.org/10.1016/j.jece.2017.11.003

Bentahar S, Dbik A, Khomri M, Messaoudi N, Lacherai A. 2018. Removal of a cationic dye from aqueous solution by natural clay. Groundwater for Sustainable Develop. (107): 1-35. https://doi:10.1016/j.gsd.2018.02.002

Brião GV, Jahn SL, Foletto EL, Dotto GL. 2017. Adsorption of Crystal Violet dye onto a mesoporous ZSM–5 zeolite synthesized using Chitin as Template. J. of Colloid and Interface Science (508): 313-322. https://doi.org/10.1016/j.jcis.2017.08.070

Bukhtiyarova MV. 2019. A review on effect of synthesis conditions on the formation of layered double hydroxides. J. of Solid State Chem. (269): 494–506. https://doi.org/10.1016/j.jssc.2018.10.018

Cai M, Su J, Zhu Y, Wei X, Jin M, Zhang H, Dong C, Wei Z. 2016. Decolorization of azo dyes Orange G using hydrodynamic cavitation coupled with heterogeneous Fenton process. Ultrason. Sonochemistry (28): 302–310. https://doi.org/10.1016/j.ultsonch.2015.08.001

Chen X & Getman RB. 2024. The Significant Differences in Solvation Thermodynamics of C1–C3 Oxygenates in Hydrophilic versus Hydrophobic Pores of a Hydrophilic Ti-FAU Zeolite Model. Journal of Physical Chemistry C (128) (45): 19367-19379. https:// DOI: 10.1021/acs.jpcc.4c04596

Chicinas R.P, Bedelean H, Stefan R, Mãicãneanu A. 2018. Ability of a montmorillonitic clay to interact with cationic and anionic dyes in aqueous solutions. J. Mol. Structure (1154): 187-195. https://doi.org/10.1016/j.molstruc.2017.10.038

Cunico P, Magdalena CP, De Carvalho TEM, Fungaro DA. 2009. Adsorption of Black Reactive Dye 5 in Aqueous Solution Using Light Coal Ash - A Review: key elements for a sustainable World Energy, Water and Climate Change. 2nd International Workshop Advances in Cleaner Production (1): 10 pp. (Cited: May 20-22, 2009) Available from: https://www.academia.edu/127864598/Adsorption_of_Reactive_Black_5_Dye_From_Aqueous_Solution_By_Coal_Fly_Ash

Danette L, Mayville A, Mayville Jr. FC. 2003. Synthesis of methyl orange using ionic liquids. Tetrahedron Letters 44(51): 9223 – 9224. https:// doi:10.1016/j.tetlet.2003.10.036

Das J, Patra BS, Baliarsingh N, Parida KM. 2006. Adsorption of phosphate by layered double hydroxides in aqueous solutions. Applied Clay Sci. 32 (3–4): 252-260. https://doi.org/10.1016/j.eti.2022.102777

De Oliveira Junior GO, Barbosa W, Da Silva ML, Carneiro DTS, De Morais JC, Ferreira LDS, Da Costa LB, Cardoso AGD. 2013. Economic, Social, and Educational Studies and Research on the Microregions of the State of Goiás – Microregion of Anápolis. Observatory of the World of Work, 53p. , Goiânia, 2nd consolidation. Available from: https://www.ifg.edu.br/attachments/article/493/microrregiao_anapolis_2%20consolidacao.pdf

Duan X, Evans DG. 2006. Layered Double Hydroxides: Structure and Bonding. Springer, Berlin/Heidelberg (119): p. 1–87. https://doi.org/ 10.1007/430_005

Effting L, Pires EL, Giona RM, Bail A. 2017. Synthesis, characterization, and evaluation of the magnetic HDL-Mg/Al adsorbent in the removal of arsenic(V) from water. 2017. TCC (Chemistry Course) - Federal Technological University of Paraná, Medianeira – PR, 59 pp. Available from: http://repositorio.utfpr.edu.br/jspui/handle/1/13248

Elmoubarki R, Mahjoubi, FZ, Elhalil A, Abdennouri HTM, Sadiq M, Qourzal S, Zouhri A, Barka N. 2017. Ni/Fe and Mg/Fe layered double hydroxides and their calcined derivatives: preparation, characterization, and application on textile dye removal. J. of Materials Res. and Technology 6 (3): 271-283. http://dx.doi.org/10.1016/j.jmrt.2016.09.007

Gilles CH, Smith D, Huitson A. 1974. General Treatment and Classification of the Solute Adsorption Isotherm - I Theoretical. J. Colloid Interface Sci. (47): 755. http://dx.doi.org/10.1016/0021-9797(74)90252-5

Goh KH. Lim TT, Dong Z. 2008. Application of layered double hydroxides for removal of oxyanions: A review. Water Research 42 (6–7): 1343–1368. https://doi.org/10.1016/j.watres.2007.10.043

Haddou B, Guitri N, Debbab A, Gourdon C, Derriche Z. 2011. Cloud Point Extraction of Orange II and Orange G Using Neutral and Mixed Micelles: Comparative Approach Using Experimental Design. Separation Science and Technology (46): 734–743. https:// doi: 10.1080/01496395.2010.535804

Hao W, Flynn SL, Alessi DS, Konhauser KO. 2018. Change of the point of zero net proton charge (pHPZNPC) of clay minerals with ionic strength. Chemge (493): 458-467. http://dx.doi.org /10.1016/j.chemgeo.2018.06.023

Henrique DC, Henrique DC, da Silva Duarte JL, Georgin J, Franco DSP, Mielli L. 2023. Transformation of Mytella falcata residual shell into CaAl/LDH adsorbent: Removal of methyl orange and methylene blue dyes. Can. J. Chem. Eng. (101)(12): 7145-7161 https://doi.org/10.1002/cjce.24948

Imgharn A, Anchoum L, Hsini A, Naciri Y, Laabd M, Mobarak M, Aarab N, Bouziani A, Szunerits S, Boukherroub R, Lakhmiri R, Albourine A. 2022. Effectiveness of a novel polyaniline@Fe-ZSM-5 hybrid composite for Orange G dye removal from aqueous media: Experimental study and advanced statistical physics insights, Chemosphere (295):133786. https://doi.org/10.1016/j.chemosphere.2022.133786.

Jadham J, Sanyal M, Joshi S, Sharma S, Sharma U. 2023. Surface Modified MgFe Layered Double Hydroxide: An Efficient Photo Catalyst for Degradation of Methyl Orange. International J. of Innovative Sci. and Res. Technology 8(2): 1627-1639. https://ijisrt.com/assets/upload/files/IJISRT23FEB1251_(1).pdf.

Jiao YN and Hou WG. 2007. Effects of structural charges on points of zero charge and intrinsic surface reaction equilibrium constants of Zn–Al and Zn–Al–Fe hydrotalcite-like compounds. Colloid Surf. A (296) (1–3): 62–66. https://doi.org/10.1016/j.colsurfa.2006.09.024

Kang J, Levitskaia TG, Park S, Kim J, Varga T, Um W. 2020. Nanostructured MgFe and CoCr layered double hydroxides for removal and sequestration of iodine anions. Chem. Engineering Journal (380): 122408. https://doi.org/10.1016/j.cej.2019.122408

Karukstis KK, Perelman LA, Wong WK. 2002. Spectroscopic characterization of azo dye aggregation on dendrimer surfaces. Langmuir (18): 10363-10371. https://doi.org/10.1021/la020558f

Kausar A, Iqbal M, Javed A, Aftab K, Nazli ZH, Bhatti HN, Nouren S. 2018. Dyes adsorption using clay and modified clay: A review. J. of Mol. Liquids (256): 395-407. https://doi.org/10.1016/j.molliq.2018.02.034

Khan AI, Raguvan A, Fong B, Markland C, O'Brien M, Dunbar TG, Willians GR, O'Hare D. 2009. Recent Developments in the Use of Layered Double Hydroxides as Host Materials for the Storage and Triggered Release of Functional Anions, Ind. Eng. Chem. Res. (48): 10196–10205. https:\\ doi: 10.1021/ie9012612

Komulski M. 2009. A pH-dependent surface charging and points of zero charge. IV. Update and new approach. J. of Colloid and Interface Sci. (337): 439–448. https:// doi.10.1016/j.jcis.2009.04.072

Komulski M. 2018. The pH dependent surface charging and points of zero charge. VII. Update. Advances in Colloid and Interface Sci. (251): 115-138. https://doi.org/10.1016/j.cis.2023.102973

Konicki W, Helminiaki A, Arabczyk W, Mijwoska E. 2018. Adsorption of cationic dyes onto Fe2+ graphite core–shell magnetic nanocomposite: Equilibrium, kinetics and thermodynamics. Chem. Engineering Res. and Design (29): 259-270. https:// doi.10.1016/j.cherd.2017.11.004

Kong F, Xie Y, Xia C, Huang H, Liang D, Qiu Y, Zhang Q, Liu X, Shao H, Meng Z. 2023. Removal of hydrogen sulfide by layered double hydroxide loaded biochar in dynamic adsorption experiment. Surfaces and Interfaces (36): 102487. https://doi.org/10.1016/j.surfin.2022.102487

Laipan M, Yu J, Zhu R, Zhu J, Smith AT, He H, O'Hare D, Sun L. 2019. Functionalized Layered Double Hydroxides for Innovative Applications. Materials Horizons 7 (3): 715–45. https:// doi: 10.1039/c9mh01494b

Leon RI, Polo CS, Ruiz JR, Fuentes EE, Fuentes ME. 2017. Study by infrared spectroscopy and thermogravimetry of the effect of temperature on nickel-aluminum hydrotalcites. Dyna 84(201): 9-16. https://doi.org/10.15446/dyna.v84n201.59768

Leont'eva NN, Cherepanova SV, Stepanova LN, Drozdov VA, Lavrenov AV. 2022. Structural Aspects of "Memory Effect" for MgGa LDHs - New Data Obtained by Simulation of XRD Patterns for 1D Disordered Crystals. Crystals 12(5): 629-643. https://doi.org/10.3390/cryst12050629

Li P, Gao B, Li A, Yang H. 2018. Highly selective adsorption of dyes and arsenate from their aqueous mixtures using a silica-sand / cationized-starch composite. J. Micro and Meso. Materials (8714): 1-35. https:// doi: 10.1016/j.micromeso.2017.12.025

Liangquan L, Jianhong B, Asfandyar S, Hua Z, Saeed R, Zhenyu W. 2024. Optimizing Mg-Fe layered double hydroxides and efficient removal of methyl orange: Screening, performance and mechanism. Environmental Technology & Innovation (34): 103629. https://doi.org/10.1016/j.eti.2024.103629

Liu YT, Wang MK, Chen TY, Chiang PN, Huang PM, Lee JF. 2006b. Arsenate sorption on lithium/aluminum layered double hydroxide intercalated by chloride and on gibbsite: sorption isotherms, envelopes, and spectroscopic studies. Environ. Sci. Technol. (40) (24): 7784–7789. http://doi.org/10.1021/es061530j

Luengo CV, Volpe MA, Avena MJ. 2017. High sorption of phosphate on Mg-Al layered double hydroxides: Kinetics and equilibrium. J. of Environmental Chem. Engineering 5 (5): 4656–4662. http://dx.doi.org/10.1016/j.jece.2017.08.051

Madhavan J. Grieser F, Ashokkumar M. 2010. Degradation of orange-G by advanced oxidation processes. Ultrasonics Sonochemistry (17): 338–343. https:// doi:10.1016/j.ultsonch.2009.10.008

Mahapatra S, Sarkar A, Tendulkar MS, Rajanayrana V. 2015. Layered Doubled Hydroxides for purification of water. World Intellectual Property Organization (WIPO/DCT) - WO 2015/193 087 A1. (Update: May 12, 2025). Available from: https://patents.google.com/patent/WO2015193087A1/en.

Mallakpour S, Motirasoul F. 2021. Adsorption of Methyl Orange from aqueous solution using PVOH composite films cross-linked by Glutaraldehyde and reinforced with modified α-MnO2. Langmuir (37): 5151-5160. https://doi.org/10.1021/acs.langmuir.1c00058

Manohara GV, Prasanna SV, Kamath PV. 2011. Structure and Composition of the Layered Double Hydroxides of Mg and Fe: Implications for Anion-Exchange Reactions. Eur. J. Inorg. Chem., pp. 2624–2630 https://doi.org/10.1002/ejic.201100104.

Mapile AN, Svensson Grape E, Brozek CK. 2024. Solvation of Nanoscale Materials. Chem. Mater. (36) (19): 9075-9088. https://doi.org/10.1021/acs.chemmater.4c01518

Maucec D, Suligoj A, Ristik A, Drazic G, Pintar A, Tusar NN. 2017. Titania versus zinc oxide nanoparticles on mesoporous silica supports as photocatalysts for removal of dyes from wastewater at neutral pH. A Review: Catal. Today (310): 32-41. https:// doi.10.1016/j.cattod.2017.05.061

Mishra G, Dash B, Pandey S. 2018. Layered double hydroxides: A brief review from fundamentals to application as evolving biomaterials. Applied Clay Sci. (153): 172-186. https://doi.org/10.1016/j.clay.2017.12.021

Mohapi M, Shale Sefadi J, Jonas Mochane M. Magagula SI, Lebelo K. 2020. Effect of LDHs and Other Clays on Polymer Composite in Adsorptive Removal of Contaminants: A Review. Crystals (10): 957. https:// doi:10.3390/cryst10110957

Murga FCG, De Campos, JDR, Signini R. 2021. Use of Aluminosilicate Residue from Insulators of High Voltage Transformers for the Adsorption of Basic Dyes. J. Braz. Chem. Soc. (00): 1-13. https://dx.doi.org/10.21577/0103-5053.20210065

Nguyen-Thanh D, Block K, Bandosz TJ. 2005. Adsorption of hydrogen sulfide on montmorillonites modified with iron. Chemosphere 59 (3): 343-353. https://doi.org/10.1016/j.chemosphere.2004.10.022

Pei YC, Wang JJ, Xuan XP, Fan J, Fan M. 2007. Factors Affecting Ionic Liquids Based Removal of Anionic Dyes from Water. Environ. Sci. Technol. (41): 5090-5095. https://doi.org/10.1021/es062838d

Rios - Leon I, Polo CS, Ruiz JR, Fuentes EE, Fuentes EM. 2017. Study by infrared spectroscopy and thermogravimetry of the effect of temperature on nickel-aluminum hydrotalcites. Dyna (84): 9-16. Available from: https://www.researchgate.net/publication/316883983

Rojas R. 2016. Effect of particle size on copper removal by layered double hydroxides. Chemical Engineering Journal (303): 331–337. http://dx.doi.org/10.1016/j.cej.2016.06.007

Rosset M, Férez LA, Perez-Lopes OW. 2022. Biogas dry reforming using Ni–Al LDH catalysts reconstructed with Mg and Zn. International J. of Hydrogen Energ, (46): 20359- 20376. https:// doi:10.1016/j.ijhydene.2021.03.150

Sato R, Machida S, Sohmiya M, Sugahara Y, Guégan R. 2021. Intercalation of a Cationic Cyanine Dye assisted by anionic surfactants within Mg−Al Layered Double Hydroxide. ACS Omega (6): 23837−23845. https://doi.org/10.1021/acsomega.1c02724

Scholtz EC, Feldkamp J R, L. White J, L. Hem S. 1985. Point of Zero Charge of amorphous Aluminum Hydroxide as a function of adsorbed carbonate. J. of Pharmaceutical Sciences (APA) 74 (4): 478-481. https://doi:10.1002/JPS.2600740423

Sheng L, Zhang Y, Tang F, Liu S. 2018. Mesoporous and microporous silica materials: Preparation from natural sands and highly efficient fixed-bed adsorption of methylene blue in waste water. J. of Micro. and Meso. Materials (257): 9-18. https://doi.org/10.1016/j.micromeso.2017.08.023

Soliman HMA & Aly HF. 2019 Hydrothermal preparation and characterization of co-based layered double hydroxide and their catalytic activity, J. Adv. Nanomater (4): 1–10, https://doi.org/10.22606/jan.2019.41001

Tavares SR, Vaiss VS, Wypych F, Leitão AA. 2014. Similarities between Zinc Hydroxide Chloride Monohydrate and Its Dehydrated Form: A Theoretical Study of Their Structures and Anionic Exchange Properties. J. of Phys. Chem. (118): 19106 −19113. https: //dx.doi.org/10.1021/jp504051z

Tichit D, Layrac G, Alvarez MG, Marcu IG. 2024. Formation pathways of MII/MIII layered double hydroxides: A review. Applied Clay Sci. (248): 107234. https://doi.org/10.1016/j.clay.2023.107234

Trujillo PG, Cruz UG, Alcaraz JFV, Soliz II, Lopez Gomes RA. 2016. Effect of Nb addition on hydrotalcite-type compounds. Innovation and Technological Development - Digital Magazine (7): 1-7. Available from: https://www.researchgate.net/profile/Israel-Ibarra-Solis-2/publication/297760159

Vo QV, Truong-Le BT, Thi Hoa N, Mechler A. 2025. The degradation of methyl orange by OH radicals in aqueous environments: A DFT study on the mechanism, kinetics, temperature and pH effects. J. of Molecular Structure (1323): 140631. https://doi.org/10.1016/j.molstruc.2024.140631

Xu ZP, Stevenson G, Qing Lu C, Qing Max Lu G. 2006. Dispersion and Size Control of Layered Double Hydroxide nanoparticles in aqueous solutions. J. Phys. Chem. B (110): 16923-16929. https://doi.org/10.1021/jp062281o

Zhang R, Liu S. 2017. Experimental and theoretical characterization of methane and CO2 sorption hysteresis in coals based on Langmuir desorption. International Journal of Coal Geology (171): 49-60. https://doi.org/10.1016/j.coal.2016.12.007

Zhang P, He T, Li P, Zeng X, Huang Y. 2019. New Insight into the Hierarchical Microsphere Evolution of Organic Three-Dimensional Layer Double Hydroxide: The Key Role of the Surfactant Template. ACS - Langmuir 35 (42): 13562-13569. https:// doi: 10.1021/acs.langmuir.9b02465

Zhou K, Xu Z. 2018. Renormalization of ionic solvation shells in nanochannels. ACS Appl. Materials & Interfaces (10): 27801− 27809. https:// doi: 10.1021/acsami.8b0923